ELSEVIER

Engineering Geology 64 (2002) 369–386

ENGINEERING GEOLOGY

www.elsevier.com/locate/enggeo

Numerical modeling of the transient hydrogeological response produced by tunnel construction in fractured bedrocks

Jorge Molinero [a,*], Javier Samper [a], Rubén Juanes [b]

[a] *E.T.S. Ingenieros de Caminos, Canales y Puertos, Universidad de A Coruña, Campus de Elviña s/n, 15192 A Corunna, Spain*
[b] *Department of Civil and Environmental Engineering, University of California at Berkeley, 631 Davis Hall, Berkeley CA 94720-1710, USA*

Received 30 May 2001; accepted 21 September 2001

Abstract

Groundwater inflows into tunnels constructed in fractured bedrocks not only constitute an important factor controlling the rate of advancement in driving the tunnel but may pose potential hazards. Drawdowns caused by tunnel construction may also induce geotechnical and environmental impacts. Here we present a numerical methodology for the dynamic simulation of the hydrogeological transient conditions induced by the tunnel front advance. The methodology is based on the use of a Cauchy boundary condition at the points lying along the tunnel according to which water discharge, Q, is computed as the product of a leakage coefficient, α, and the head difference, $(H-h)$, where H is the prescribed head at the tunnel wall and h is the hydraulic head in the fractured rock in the close vicinity of the tunnel. At a given position of the tunnel, α is zero until the tunnel reaches such position when it is assigned a positive value. The use of step-wise time functions for α allows an efficient and accurate simulation of the transient hydrogeological conditions at and around the tunnel during the excavation process. The methodology has been implemented in TRANMEF-3, a finite element computer code for groundwater flow in 3D fractured media developed at the University of A Coruña, Spain, and has been used to simulate the impact of a tunnel on the groundwater system at the Äspö island (Sweden). This tunnel was constructed to access an underground laboratory for research on radioactive waste disposal. The large amount of available data at this site provides a unique opportunity to test the performance of the numerical model and the proposed methodology for tunnel advance. With just minor calibration, the numerical model is able to reproduce accurately the measurements of inflows into the tunnel at several reaches and hydraulic heads at surface-drilled boreholes. These results obtained at the Äspö site lead us to conclude that accurate predictions of the transient hydrogeological responses induced by tunneling works in fractured bedrocks, can be achieved provided that a sound hydrogeological characterization of large-scale fracture zones is available.

Keywords: Numerical modeling; Tunneling; Groundwater inflows; Inner-moving boundaries; Fractured rocks; Äspö island

1. Introduction

Groundwater inflows into tunnels may constitute a potential hazard as well as an important factor controlling the rate of advancement in driving a tunnel. One of the major practical difficulties often associated with tunnel construction is related to groundwater. In fact, some of the most disastrous experiences in tunneling have been the result of interception of large flows of water from highly fractured water-saturated rocks (Freeze and Cherry, 1979). In addition, predic-

* Corresponding author. Fax: +34-981-16-71-70.
E-mail address: molinero@iccp.udc.es (J. Molinero).

0013-7952/02/$ - see front matter
PII: S0013-7952(01)00099-0

tions of groundwater inflows are needed to design suitable drainage systems. As shown by Jansson (1979), a dramatic increase in tunnel-driving cost in fractured granites is related to water inflows occurring at large permeability zones. On the other hand, drawdowns produced by tunnel construction may induce land subsidence, water table decline and environmental impacts on rivers and wetlands.

There are several analytical expressions in the literature to calculate discharges into tunnels. In a homogeneous infinite watertable aquifer, the flow rate per unit tunnel length, q, can be obtained from the semi-log Jacob approximation of drawdown as proposed by Goodman et al. (1965):

$$q = \frac{2\pi K H_o}{\ln(2H_o/r)} \quad (1)$$

where K is hydraulic conductivity, r is radius of the tunnel and H_o is the depth of the axis of the tunnel below the water table. Eq. (1) is known in the scientific literature as the 'large well formula' (Galperin et al., 1993). Galperin et al. (1993) used it to derive a set of expressions to compute tunnel inflows in bounded semi-infinite aquifers for several combinations of constant head and/or impervious boundaries.

On the other hand, drawdowns produced in a watertable aquifer due to the excavation of a tunnel can also be evaluated analytically. The drawdown, s, at a horizontal distance, L, of a tunnel having a radius r much smaller than its length is given by (Custodio, 1983):

$$s = \frac{q}{2\pi K}\left[\frac{\pi L}{b} - \ln\left(\frac{2\pi r}{b}\operatorname{sen}\frac{\pi a_b}{b}\right)\right] \quad (2)$$

where q is the flow rate into the tunnel, b is aquifer thickness and a_b is the distance from the axis of the tunnel to the bottom of the aquifer.

Bear et al. (1968) and Custodio (1983) present analytical expressions of drawdowns caused by tunnels for other hydrogeological conditions including areal recharge on the top boundary.

Analytical solutions rely on assumptions which are rarely met by fractured rocks, mainly because groundwater flow in such media takes place mostly along preferential paths of complex geometries, such as fractures and fracture zones. One must resort to numerical models to study groundwater flow in such complex hydrogeological conditions.

A numerical flow model is a simplified representation of an aquifer which aims at capturing the most relevant features of groundwater flow. Constructing a numerical model requires formulating first the conceptual model, which is a qualitative description of the main properties of the flow system. Several conceptual models have been proposed for water flow through fractured media (Carrera et al., 1990; Bear, 1993 and Berkowitz, 1994) which include: (1) equivalent porous media (EPM) models, (2) discrete fracture networks (DFN) models and, (3) hybrid models. EPM models are based on the assumption that flow through fracture media obeys the same laws as those of flow through porous media. This assumption is valid as long as it is possible to define a representative elementary volume (REV) (see Bear, 1993), which requires the model domain being much greater than the average distance between fractures. In DFN models the flow is assumed to occur within a finite set of connected fractures. Although these models have provided fundamental understanding on the behavior of solute transport processes (Berkowitz, 1994), their use in field problems is limited by the difficulties in defining the geometry of fracture sets. Hybrid or mixed models combine the main features of EPM and DFN models. They consider a continuum representation of the fractured domain and a discrete representation of the major fracture zones within the formation, allowing for the interaction between fracture zones and an equivalent porous domain. Hybrid models have been used successfully for simulating pumping and tracer tests in fracture media (Carrera et al., 1990, 1996; Fillion and Noyer, 1996; Gylling et al., 1998). Kiraly (1987) and Juanes et al. (2001) used finite element hybrid models to simulate flow and solute transport. Juanes et al. (2001) demonstrate that accurate and efficient numerical solutions are obtained when discrete fractures are discretized with 2D elements embedded within a 3D porous domain.

Most countries throughout the world are considering deep underground storage facilities for long-term disposal of high level radioactive waste. Low permeability geological formations such as granites, salts, tuffs and clays are being considered as candidate materials. Underground research laboratories have been constructed in several countries in order to perform basic research and demonstrate the feasibility of these repositories. The Äspö Hard Rock Laboratory

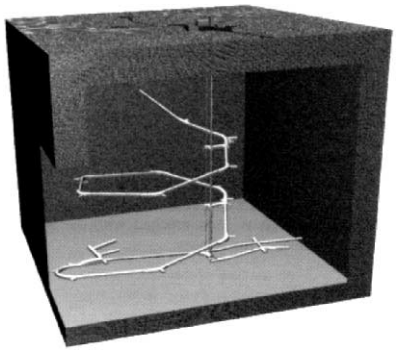

Fig. 1. General layout of the Äspö Hard Rock Laboratory. The total length of the tunnel is 3600 m. The spiral part of the excavation is connected to the Äspö Research Village by a hoist shaft and two ventilation shafts (after Rhén et al., 1997a).

(Äspö HRL) is an underground research laboratory in crystalline bedrock launched and operated by the Swedish Nuclear Waste Management Company (SKB). Construction of the Äspö facility started in October 1990 and the laboratory was completed in the summer of 1995. The underground facilities of the Äspö HRL consist on a 3600-m long tunnel that starts with an access ramp and runs in two turns down to a depth of 450 m under the Äspö island. Surface and underground facilities are connected by a hoist shaft and two ventilation shafts (Figs. 1 and 2). Data collected during the construction and operation of the Äspö HRL have been used for site characterization and model testing within the context of international research projects. One of such projects, *the Äspö Task Force on Modelling Groundwater Flow and Solute Transport* (Ström, 1996), is a forum for the organizations involved in the laboratory to interact in relevant issues related to conceptual, mathematical and numerical modeling of groundwater flow and solute transport in fractured rock. Groundwater is important for performance assessment of radioactive waste disposal, and the chemical conditions will also influence the time the waste remains isolated and the rate of any radionuclide release. The Äspö Task Force #5 project aimed at testing the capabilities of groundwater flow and hydrochemical models to predict the impact of the construction of the access tunnel on the prevailing

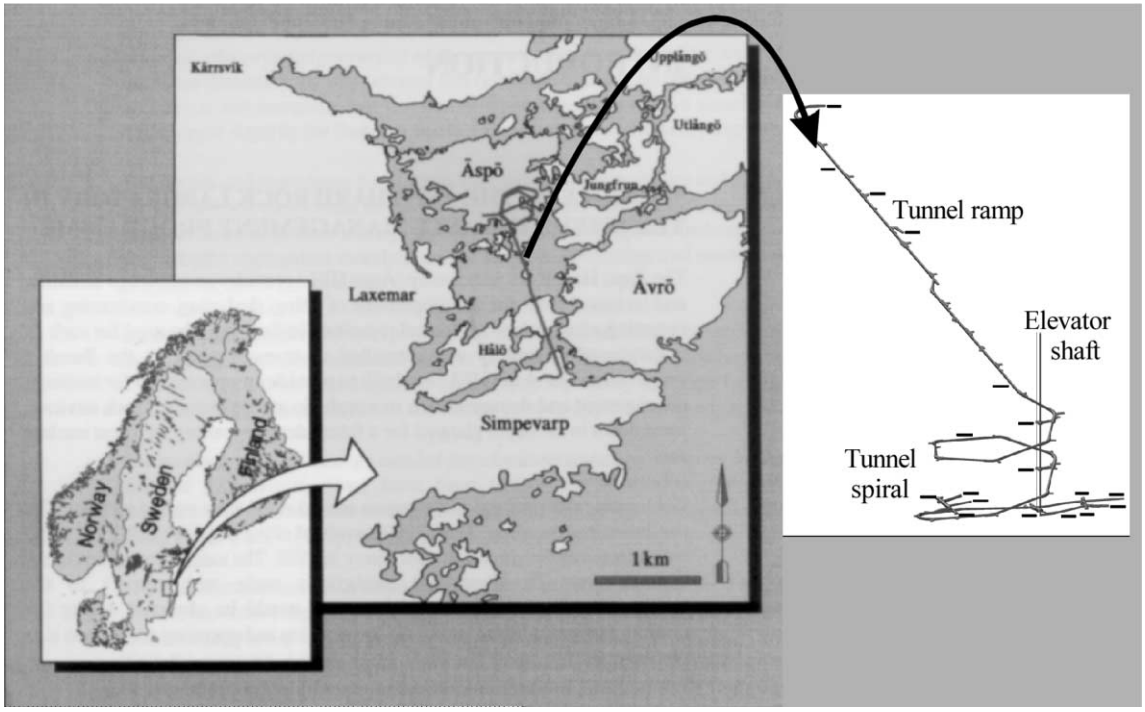

Fig. 2. Location of the Äspö Hard Rock Laboratory and a 3D view of the underground facilities (tunnel and elevator) (modified after Rhén et al., 1997b).

hydrogeological and hydrochemical conditions at the site (Wikberg, 1998). Teams from several countries contributed to this project by using various conceptual and numerical approaches.

This paper describes the Spanish contribution to the Äspö Task force #5 (Molinero, 2000; Molinero et al., 2000) which took place through ENRESA (the Spanish counterpart of SKB). A finite element model of the hydrogeology of the Äspö site was constructed using a discrete fracture approach. The model accounts explicitly for the process of tunnel construction in a rigorous and efficient manner by treating the

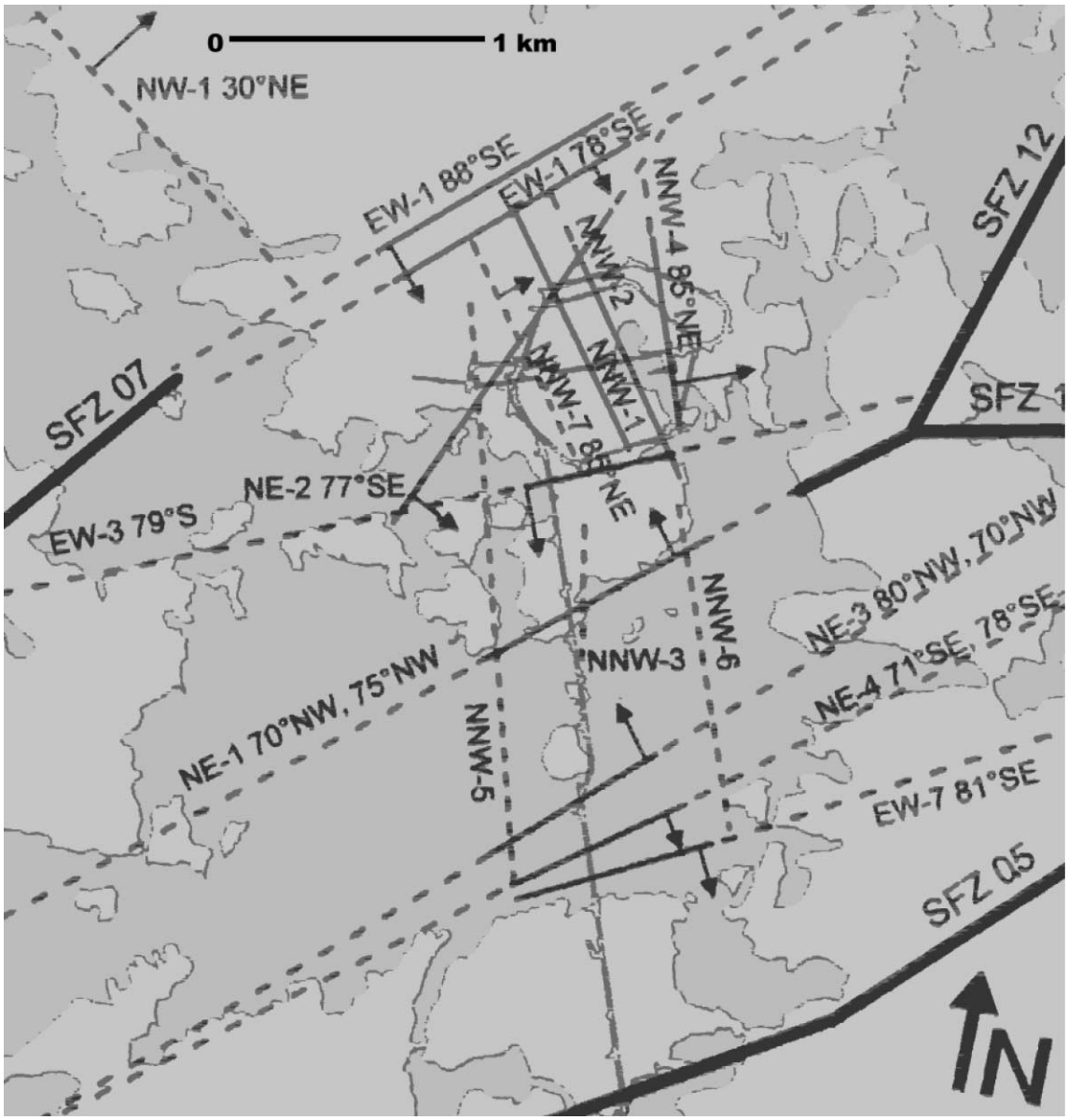

Fig. 3. Major water-conducting fracture zones identified at the Äspö site (modified after Rhén et al., 1997b). Solid lines: certain structures. Dashed lines: probable structures.

tunnel face as a time-varying inner boundary. Nodes lying along the tunnel are assigned a Cauchy-type boundary condition in the finite element model. It is shown that by using this type of boundary condition there is no need to use moving grids for simulating the transient hydrodynamic regime induced by the advance of the tunnel front.

The main hydrogeological features of the Äspö area are described first. Then, conceptual and numerical models of groundwater flow are shown. Details of the implementation of the time-varying inner boundary condition for the tunnel are also provided. Finally, the results of model calibration and testing as well as a discussion of the main achievements are presented.

2. Äspö HRL site description

The Äspö island is surrounded by the Baltic Sea, in the southeast part of Sweden, 400 km south of Stockholm. The island is separated from the mainland and several other islands by shallow estuaries (Fig. 2). The main rocks of the area are granitoids of the Transscandinavian Igneous Belt. They were emplaced and extruded during several pulses of Precambriam magmatism (Larson and Berglund, 1992). Their mineralogical composition range from true granites, which occur at Ävrö island and the southern part of Äspö (Fig. 2), to granodiorites and diorites in the northern part of Äspö (Kornfalt and Wikman, 1988). U–Pb isotopic data indicate that the intrusion of these granites took place between 1760 and 1840 Ma ago (Banwart et al., 1999).

The land surface of Äspö is slightly undulating with a maximum height of 14 m a.s.l. There are not perennial streams on the island. Surface waters are drained directly to the sea and through peatlands and shallow sediments. The mean annual precipitation in the area is about 675 mm, 18% of it occurs as snow. Calculated actual evapotranspiration (ET) is 490 mm/year while potential ET is 616 mm/year (Rhén et al., 1997a,b). The average temperature is 6.5 °C. Groundwater recharge ranges from 5 to 35 mm/year (Banwart et al. 1999).

The water table is shallow and mimics approximately the topographic surface. Under natural conditions its elevation ranged between 0 and 4 m a.s.l.

Table 1
Hydraulic conductivity, storativitiy and thickness of the major fracture zones according to Rhén et al. (1997b). Fracture zones are denoted by their orientation and numbering adopted in this study

Fracture zone number	Fracture zone I.D.	Thickness (m)	Geometric mean of the measured hydraulic conductivity (m/day)	Confidence limit (2.5%) (m/day)	Confidence limit (97.5%) (m/day)	Sample size (–)	Measured storativities (m^{-1})
1	EW–1N	30	4.32×10^{-3}	4.32×10^{-6}	5.18×10^{-1}	4	
2	EW–1S	30	6.34×10^{-2}	4.90×10^{-4}	2.53	4	
3	EW-3	15	1.38×10^{-1}	1.38×10^{-2}	6.91×10^{-1}	4	
4	EW-7	10	5.88×10^{-1}	8.64×10^{-5}	$1.81 \times 10^{+2}$	3	
5	NE-1	30	8.64×10^{-1}	3.46×10^{-1}	1.21	16	8.66×10^{-7}
6	NE-2	5	7.08×10^{-3}	9.46×10^{-5}	4.84×10^{-2}	12	
7	NE-3	50	5.01×10^{-1}	2.42×10^{-1}	1.24	9	
8	NE–4N	40	6.48×10^{-2}	1.47×10^{-2}	3.02×10^{-1}	8	
9	NE–4S	40	6.48×10^{-2}	1.47×10^{-2}	3.02×10^{-1}	8	
10	NNW-1	20	4.75×10^{-2}	3.24×10^{-3}	1.06×10^{-1}	7	2.50×10^{-7}
11	NNW-2	20	2.42×10^{-1}	5.62×10^{-4}	$1.90 \times 10^{+1}$	4	1.00×10^{-7}
12	NNW-4	10	1.30	1.56×10^{-2}	5.18	8	
13	SFZ-11	20					
14	NW-1	10	1.47×10^{-3}	2.85×10^{-4}	4.23	3	
15	NNW-5	20	8.64×10^{-3}	2.72×10^{-3}	3.84×10^{-1}	3	
16	NNW-6	20					
17	NNW-7	20	2.07×10^{-2}	1.77×10^{-2}	7.78×10^{-2}	5	
18	NNW-8	20	4.32×10^{-2}	3.63×10^{-6}	8.64×10^{-1}	3	
19	NNW-3	20					

and decreased significantly during tunnel construction reaching a minimum of about −100 m a.s.l. in 1995. Since then it has remained more or less stable (Stanfors et al., 1999).

Geological, geophysical and hydrogeological studies performed before and during tunnel construction (from 1986 to 1995) provided a detailed characterization of the geology and hydrogeology of the site (Rhén et al., 1997a,b).

The geological model of the site was derived from airborne magnetic, electromagnetic and radiometric measurements. Lineament interpretation of terrain models was used to identify major fracture zones (Rhén et al., 1997a). Surface petrophysical measurements of rock samples and ground geophysics (gravity and refraction seismic mainly) also revealed anomalies that were identified as fracture zones (Rhén et al., 1997b). In addition, an extensive drilling program with geophysical logging was carried out, including VLF electromagnetic, resistivity, magnetic, radiometric and borehole radar (Rhén et al., 1997a). Detailed geological mapping of surface bedrock was also carried out.

A large number of hydraulic tests were performed to characterize the hydrogeological parameters of fracture zones. The major conductive fracture zones are shown in Fig. 3. Two main trends can be identified in this figure. There is a first group of fracture zones trending NE–SW and E–W (identified as NE and EW, respectively), and a second group of NNW–SSE trending features (identified as NNW in Fig. 3).

Hydraulic tests were performed using packer-isolated intervals of 3, 30 and 100 m. Transmissivities of fracture zones range from 10^{-6} to 10^{-4} m^2/s with a median of 10^{-5} m^2/s (Table 1). The largest value of 3×10^{-4} m^2/s was measured at fracture zone NE-1 (see Fig. 3 and Table 1). Fracture zone thickness ranges from 10 to 50 m. Hydraulic conductivities of the surrounding rock mass domains (outside of the fracture zones) have a mean value of 3×10^{-10} m/s (Rhén et al., 1997b). Therefore, major water-conducting fracture zones have hydraulic conductivities which are from 3 to 5 orders of magnitude larger than those of the rock domains. Storativity data were determined from interference hydraulic tests (see Table 1). Contrary to what has been observed at other Swedish granitic basements hydraulic conductivity in the Äspö area does not decrease with depth, at least to a depth of −600 m a.s.l. (Stanfors et al., 1999). However, in the nearby area of Laxemar (located in the mainland of the Baltic Coast; see Fig. 1) a 1700-m deep cored borehole indicated a significant decrease in hydraulic conductivity at depths ranging from −700 to −1000 m a.s.l.

Groundwater chemistry was studied in several boreholes by using a mobile field laboratory with

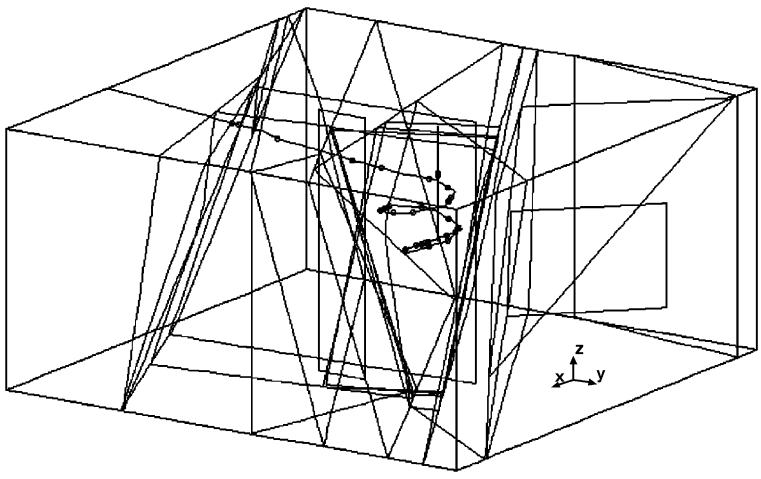

Fig. 4. Model domain geometry including all major water-conducting fracture zones defined at the Äspö site, the tunnel and the elevator. Points represent the intersections between tunnel (and elevator shaft) and fracture zones.

downhole measuring devices as well as by sampling during pumping tests. Shallow groundwaters (0–150 m) are of Na–Ca(Mg)HCO_3–Cl type. Waters from 300- to 800-m depths are of Na–Ca(Mg)Cl–SO_4 type. Below 800-m depth, groundwaters are saline and mostly of Ca–Na(Mg)Cl–SO_4 type (Smellie et al., 1995). The concentrations of Cl, Br, Na, Ca, SO_4, Sr and Li increase with depth while the concentrations of others species such as HCO_3, Mn, Mg, $Fe_{(tot)}$ and TOC (total organic carbon) show a reverse trend (Smellie et al., 1995). The fresh water lens in the Äspö island reaches a maximum depth of -200 m a.s.l. (Rhén et al., 1997b). There is a zone of brackish waters (from 0 to 8 g/l of Cl^-) from -200 to almost -800 m a.s.l. High-salinity waters (up to 45 g/l of Cl^-) are present below -800 m a.s.l. These saline waters remained virtually stagnant for the last 1.5 Ma (Louvat et al., 1999).

Additional details on the overall geo-hydrological regime of the Äspö site can be found in Stanfors et al. (1999) and Smellie et al. (1995).

3. Conceptual model

The comprehensive geological and hydrogeological research activities performed at the Äspö site allowed the identification and characterization of the major water-conducting fracture zones. Groundwater flow system in the Äspö island is controlled by these major fracture zones (Smellie et al., 1995). The largest flow rates into the tunnel occur at sections where major fracture zones are intersected. The hydrogeological model of the Äspö site calls for a discrete fracture network model in which the role of rock mass domains can be neglected. For this reason, a numerical model containing only the major fracture zones was adopted. The fact that computed heads and fluxes match recorded measurements is a posteriori confirmation of the plausibility of this assumption.

The fracture network contains the 19 major water-conducting fracture zones detected at Äspö (Fig. 4). This fracture network is located within a three dimensional block of 2×2 km^2 upper surface and 1 km depth (Fig. 4). Eleven fracture zones are intersected either by the tunnel or by the elevator. It should be noticed that the spiral part of the tunnel intersects some fracture zones more than once (Fig. 4).

Groundwater flow through fracture zones occurs under full saturation conditions and is governed by the aquifer flow equation:

$$\nabla \cdot (\underline{\mathbf{T}} \nabla h) + r = \boldsymbol{S} \frac{\partial h}{\partial t} \tag{3}$$

where $\underline{\mathbf{T}}$ is transmissivity tensor, $\boldsymbol{S}$ is storativity, $\nabla\cdot(\,)$ and $\nabla(\,)$ are the divergence and gradient operators, respectively, r is a sink/source term of water per unit surface, t is time and h is piezometric head.

Initial values of piezometric heads, h_o, are either known or obtained from the solution of a steady-state flow equation. In the Äspö site model, initial heads are

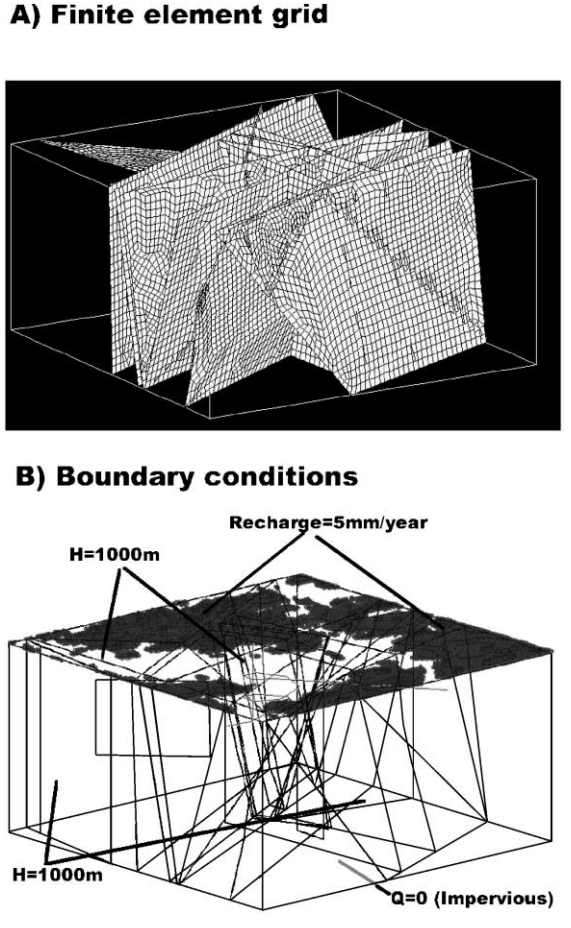

Fig. 5. (A) Finite element grid used for the spatial discretization of major water-conducting fracture zones. (B) Sketch of the boundary conditions of the numerical model.

assumed to be hydrostatic. On the boundary of the flow domain, Γ, either heads or water fluxes are known. Possible boundary conditions include,

(1) Dirichlet condition:

$$h(x,y,z,t)\,|_{\Gamma_1} = H \tag{4}$$

where Γ_1 is the portion of Γ where head is prescribed to a value H.

(2) Neumann condition:

$$\underline{\mathbf{T}}\nabla h \cdot \vec{\mathbf{n}}\,|_{\Gamma_2} = Q \tag{5}$$

where Γ_2 is the portion of Γ with a prescribed flux Q and $\vec{\mathbf{n}}$ is a unit vector perpendicular to the boundary and pointing outwards.

(3) Cauchy (mixed) condition:

$$\underline{\mathbf{T}}\nabla h \cdot \vec{\mathbf{n}}\,|_{\Gamma_3} = \alpha(H - h) \tag{6}$$

where Γ_3 is the portion of Γ across which the flux is equal to the product of a leakage coefficient, $\alpha(LT^{-1})$, and the head difference $(H - h)$.

Hautojärvi et al. (1994) showed that the effect of water density variations in groundwater pressures is negligible at the Äspö site, once the system is altered by the tunnel construction. Water pressures are mostly controlled by the hydraulic gradient induced by the tunnel construction. For this reason, density changes caused by variations in water salinity were disregarded.

Hydrodynamic parameters of each fracture zone are assumed to be homogeneous, isotropic and constant in time (Table 1).

4. Numerical model

The model domain was discretized using 2D quadrilateral and triangular finite elements in fracture zones (Fig. 5). 1D linear elements were used for fracture intersections, the Äspö HRL tunnel and the elevator (Fig. 5). The finite element mesh contains 12,847 nodes and 14,273 elements.

Numerical simulation covers a period of 2013 days starting on June 27, 1991, just after the tunnel intersected the first fracture zone (EW-7) and ending on January 1, 1997. For the most part, constant time steps, Δt, of 1 day were used. In order to capture properly the fast transient hydraulic responses of fracture zones when they are intersected by the tunnel, smaller time steps of $\Delta t = 0.1$ day were used for several days after the tunnel intersected each fracture zone.

Initial hydrostatic conditions were adopted throughout the model. It is worth noting that the maximum elevation of the water table at the island was about 4 m a.s.l prior to tunnel excavation. To facilitate numerical model pre-processing, the system of coordinates was placed at a depth of 1,000 m below sea level (at the bottom of the domain). Then, initial heads are everywhere equal to 1000 m.

The granite is assumed to be impervious at a depth of 1 km. Heads were prescribed at their initial values along the side boundaries. A Dirichlet condition was also used for nodes lying on the Baltic Sea with a fixed head of 1000 m. A Neumann condition of specified groundwater recharge was used for the

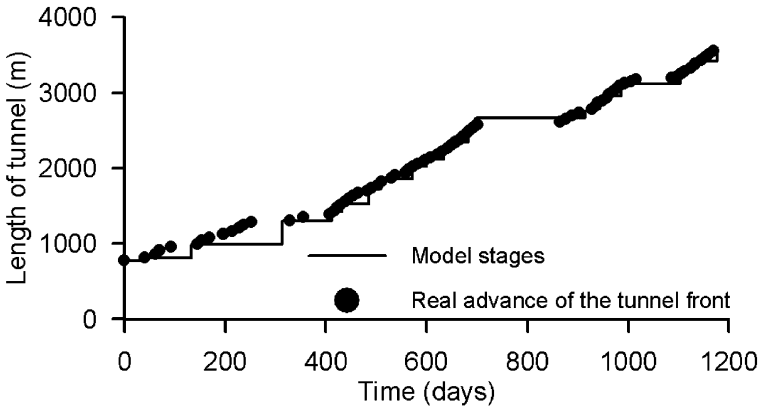

Fig. 6. Actual tunnel front advance (points) and model stages used to simulate tunnel construction (solid line).

nodes lying on the ground surface (islands) of the top boundary. The value of the groundwater recharge was prescribed to be equal to the equivalent flow rate resulting from the assumption of a recharge of 5 mm/year in the island surface, concentrated at the outcrops of fracture zones. These outcrops constitute topographic depressions on the island. Fig. 5 shows a sketch of the adopted boundary conditions for the numerical model.

The numerical model of the Äspö site was solved with an in-house finite element code, TRANMEF-3 (Juanes, 1997; Juanes and Samper, 2001; Juanes et al., 2001). This code solves for groundwater flow, weakly reactive multicomponent solute transport and heat transfer in heterogeneous fractured formations. It uses the Galerkin finite element method for spatial discretization and the Euler finite difference scheme for time discretization. The code incorporates a rigorous formulation for boundary conditions (Juanes et al., 2001). TRANMEF-3 handles up to six different types of 1-, 2- and 3D elements that can be combined simultaneously. Elements may have different dimensions, thus allowing one to account for 1D features, such as wells, fracture intersections and tunnels, and 2D objects, such as fracture networks, embedded within a 3D medium. Numerical integration in elements and along element faces is performed by using Gaussian quadrature.

5. Simulation of tunnel construction

The advance of the tunnel front was simulated by means of 29 stages, corresponding to intersections of the tunnel with fracture zones. Fig. 6 illustrates the actual progress of the tunnel front and its numerical approximation by means of a step-wise function.

A relevant feature of the model is its ability to cope with inner-moving boundaries such as the tunnel front advance during the excavation. The code allows one to switch dynamically the type of boundary condition at the nodes lying along the tunnel. This makes possible to model the construction of the tunnel in a single computer run. The switch of boundary condition is performed by using a time-dependent mixed (Cauchy) boundary condition (Eq. (6)), in which the leakage coefficient, α, varies with time. This coefficient is initially set equal to zero at all nodes lying along the tunnel. This condition is equivalent to a no-

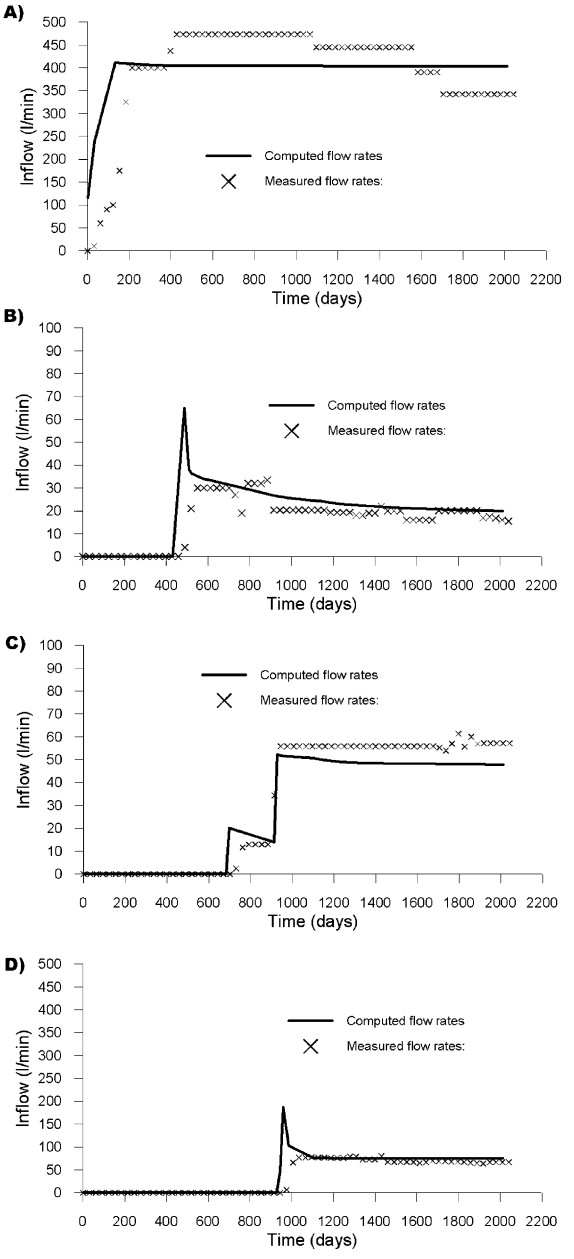

Fig. 7. Comparison of computed (solid line) and measured (symbols) flow rates at 4 of the 14 tunnel control sections: (A) 1030 m from the tunnel access; (B) 1745 m from the tunnel access; (C) 2699 m from the tunnel access; (D) 2994 m from the tunnel access.

flow boundary condition. When the tunnel front reaches a node, its leakage coefficient is assigned a large positive value, therefore imposing a prescribed external piezometric head (see Eq. (6)), which is equal to the elevation of the node. It should be noticed that water pressure in the tunnel is equal to atmospheric pressure and therefore the pressure head is zero. The time variation of leakage coefficients is achieved by means of Heaviside step-wise time functions. Their steps take place at different times for each node. The use of these functions provides a powerful procedure for simulating inner-moving boundaries and allows one to perform a fully dynamic simulation of the advance of the tunnel front.

6. Model results

6.1. Inflows into the tunnel

Inflows into the tunnel were gauged along a number of tunnel intervals most of which contain major fracture zones. Measured inflows at 14 intervals were used to estimate hydraulic conductivities and storativities of fracture zones by trial-and-error calibration. Computed inflow hydrographs match the measured values at all these intervals. Fig. 7 shows the results obtained at four of such control intervals.

Fig. 8 shows the time evolution of the cumulative water inflow into the tunnel. The model reproduces the trend of measured flow rates because they are controlled mainly by the intersections between the tunnel and the major water-conducting fracture zones. Even though the model reproduces the flow rates at most control sections, model results underestimate the total amount of water flowing into the tunnel, especially in the period from 800 to 1200 days, when a maximum discrepancy of about 20% is observed (see Fig. 8). Later, these discrepancies decrease and become less than 5% when steady state is reached after 1500 days. It should be noticed that our numerical model does not account for water flow through the rock blocks between the major fracture zones. Therefore, computed flow rates are expected to be smaller than measured values. Inasmuch as computed inflows match measured data at control sections containing major conductive features, the role of the rock blocks between fracture zones can be evaluated from the comparison of computed and measured cumulative flow rates (Fig. 8). It can be stated that rock blocks contribute approximately 20% of the total amount of water flowing into the tunnel during the transient stage. This contribution, however, decreases gradually to less than 5% at steady state. This analysis indicates that granite blocks at the Äspö site show a noticeable storage capacity, but a small ability to transmit water. The storage capacity of a fractured rock depends mostly on its fracture density while its transmissivity depends on the density and connectivity of the fracture network. It can be concluded that meso-fractures (metric scale) within rock blocks are poorly connected at the Äspö site. In summary, the

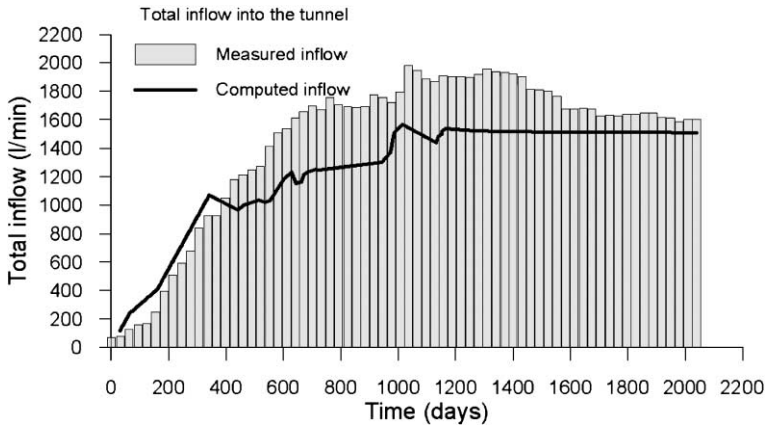

Fig. 8. Comparison of computed and measured cumulative water inflow into the total length of the excavation.

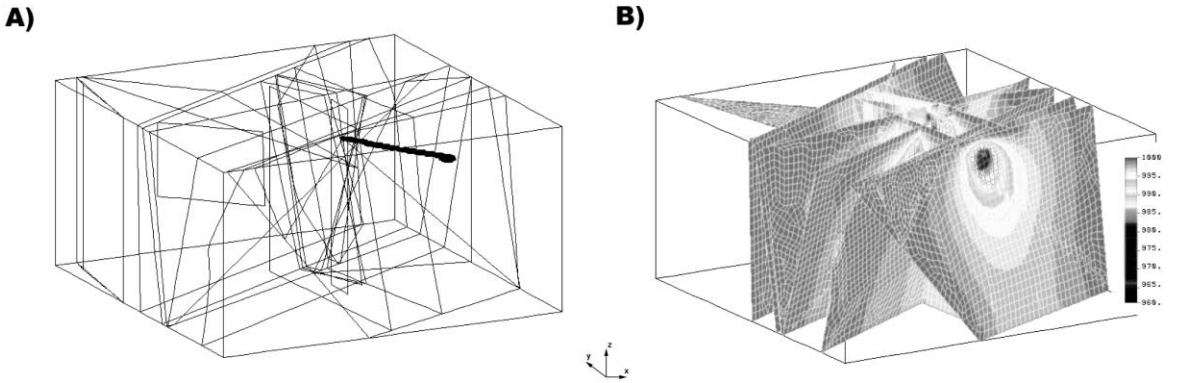

Fig. 9. 3D view of: (A) fracture zones and tunnel front position at 1531 m from the starting point, and (B) computed hydraulic heads (m) after 432 days.

accurate simulation of the transient tunnel advance is responsible for the excellent agreement achieved between measured and computed flow rates, at each one of the control points (Fig. 7), as well as the match in the trend of the cumulative time evolution of the tunnel inflows (Fig. 8).

6.2. Groundwater heads and water table

Figs. 9 and 10 show 3D views of computed heads after 423 and 2013 days, respectively. These figures illustrate the transient evolution of hydraulic heads in response to the construction of the tunnel. As expected, computed piezometric contours show a more or less concentric pattern around the tunnel thus indicating that the tunnel acts as a groundwater sink.

Hydraulic heads were monitored at 15 control points corresponding to isolated (packed) sections of surface-drilled boreholes crossing one or more fracture zones. Data monitored during the first 800 days were used for model calibration. After calibration, numerical results reproduce the trends of measured head hydrographs as one can see in Fig. 11 which shows the fit of computed values to measured heads at three of the control points. Measured data after 800 days were used to test the validity of the model. Computed heads reproduce measured field data during both the calibration and validation stages (Fig.

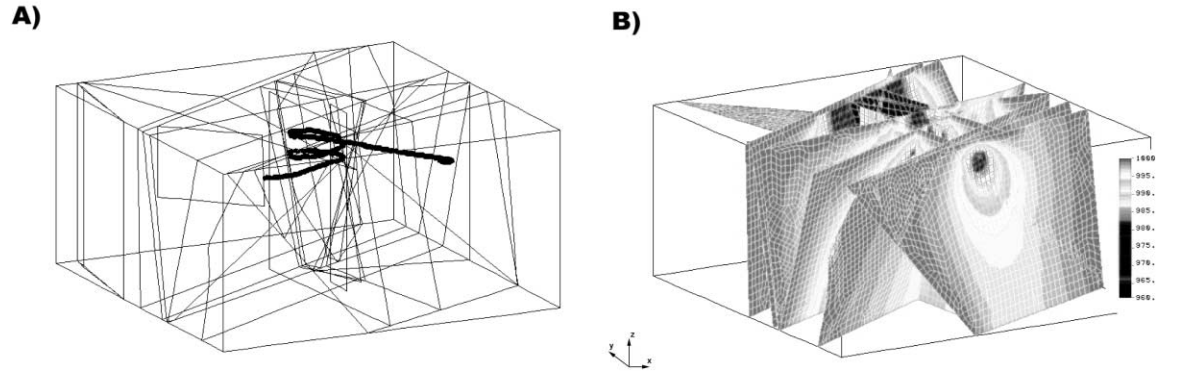

Fig. 10. 3D view of the computed hydraulic heads (m) after 2013 days (2 years and 3 months after tunnel completion). This hydraulic head distribution corresponds to the quasi steady-state tunnel-disturbed system. Also shown on the left is the tunnel front position at 3600 m from the starting point (the total excavation length).

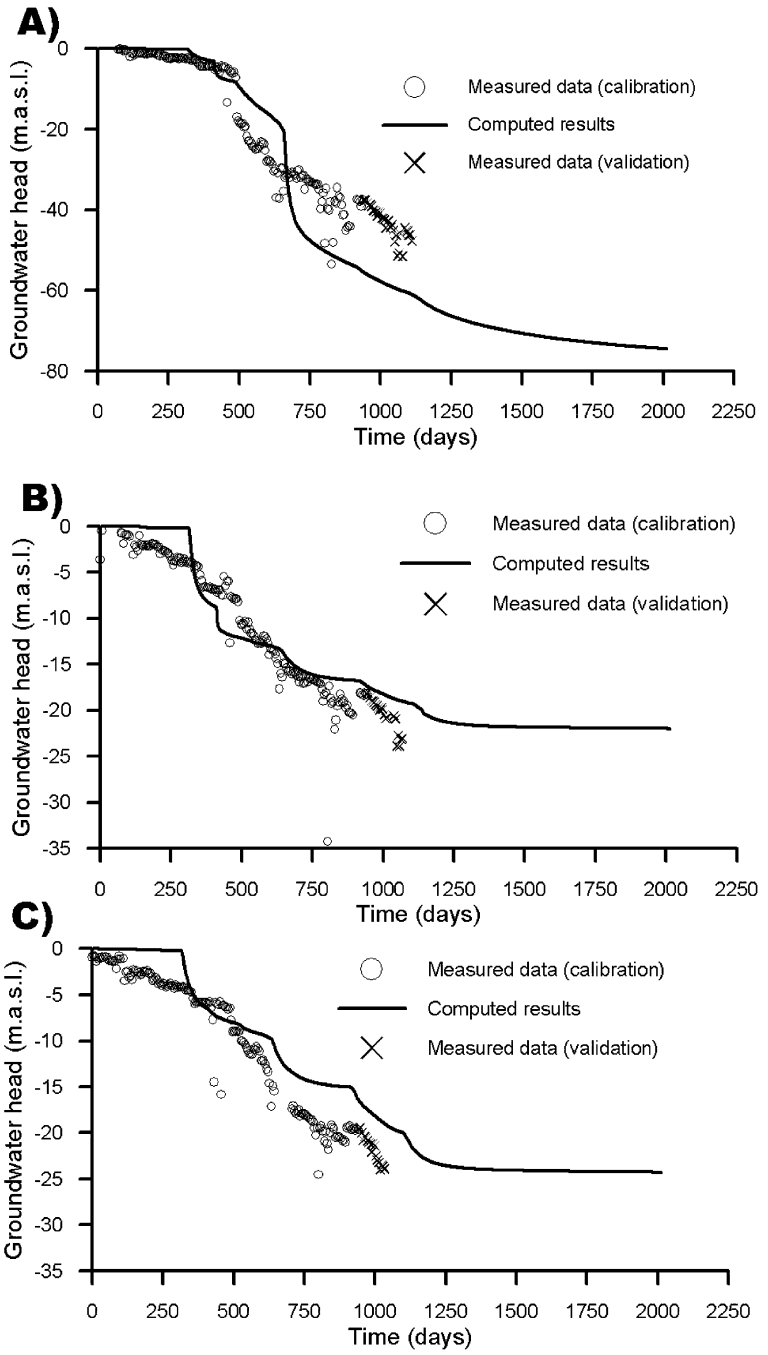

Fig. 11. Comparison of computed (solid line) and measured (symbols) heads at three surface-drilled boreholes. Depths of the packed sections for measurements are: (A) 191–290 m; (B) 501–604 m; (C) 503–601 m.

11). Although computed heads reproduce reasonably well the trends of measured data, the former tend to show sharper/steeper responses than the later. This can be seen in Fig. 11. While the evolution of computed heads shows a step-like drawdowns, measured heads evolve in a smoother manner. This step behavior of computed heads evolution is discussed in the next section.

To quantify the quality of the fit of computed heads, h^c, to measured heads, h^m, the mean absolute value of head residuals (dh_{abs}) was calculated according to:

$$dh_{abs} = \frac{\sum_{i=1}^{n} | h_i^m - h_i^c |}{n} \quad (7)$$

where n is the number data. The mean absolute value of head residuals was computed at different times during tunnel construction. Fig. 12 shows the time evolution of the mean residual during both calibration and validation stages. At early times, the mean residual increases with time because the number of control points also increases. It attains an average value of 2 m within the interval 200–500 days. Then, it increases up to 5 m at the end of the calibration stage. It should be noticed that head residuals after 800 days oscillate about the same mean value as that of the late stages of calibration.

Fig. 13 shows a comparison of measured and computed water table contour maps at 2 different times during the tunnel construction process. Both computed and measured contour maps were interpolated by using a kriging technique. A plan view of the tunnel front position is also shown in order to illustrate the transient impact of the tunnel construction on the water table of the Äspö island. Computed water table (Fig. 13B and D) show a more discontinuous pattern than measured maps (Fig. 13A and C). An important difference between both maps is that computed results show two zones with maximum drawdowns (Fig. 13D), while measured water table show just one (Fig. 13C). The discontinuous pattern of computed water table is due to the influence of several NNW fracture zones outcropping at the Äspö island (see Fig. 3 for the location of fracture zones). However, the effect of the NNW fracture zones is not reflected so clearly in the measured water table map due to the fact that there are not enough observation boreholes in some parts of the island. Fig. 13F shows the nodes of the finite element grid lying at the surface, which are used to interpolate the computed water table map. On the other hand, Fig. 13G shows the location of surface drilled boreholes on the Äspö island used to interpolate the measured water table map. It can be seen in this figure that the two main discrepancies between computed and measured inter-

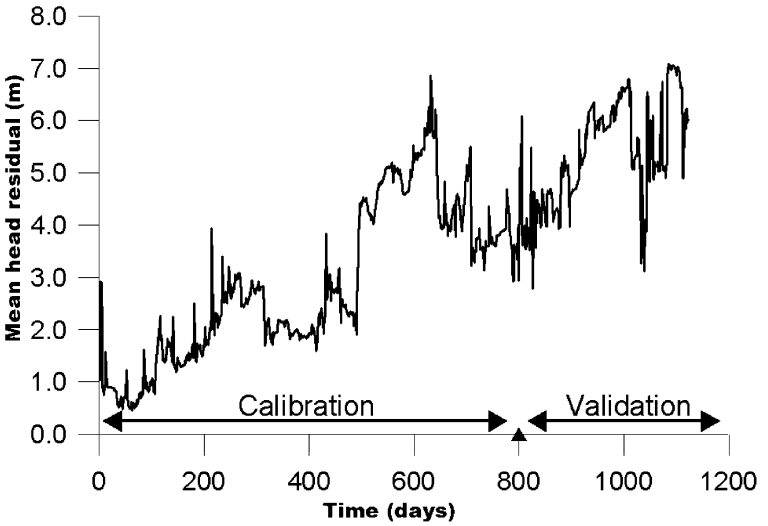

Fig. 12. Time evolution of the mean absolute value of head residuals during both calibration and validation stages.

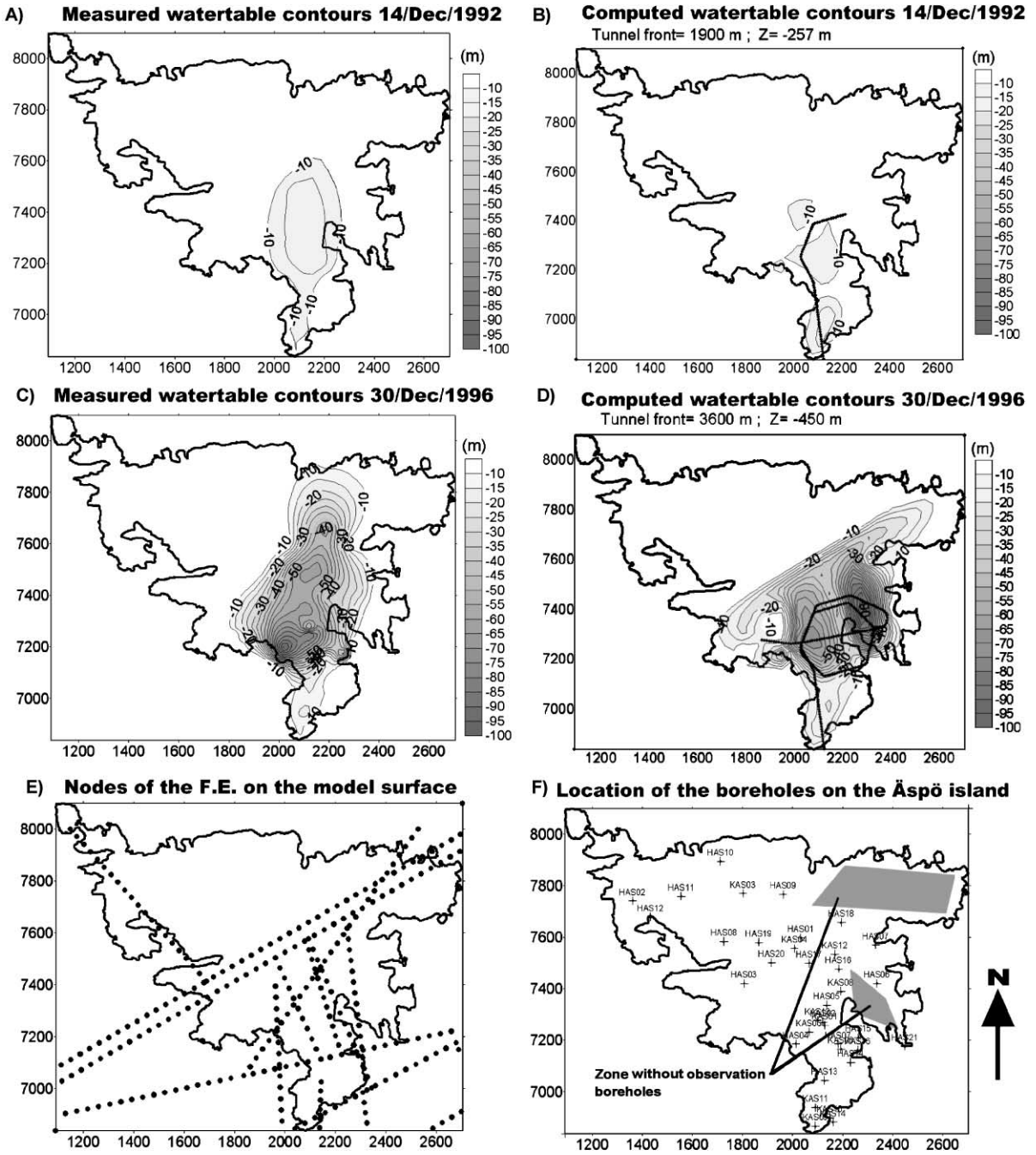

Fig. 13. Kriged water table contour maps (m a.s.l.) of: (A) measured values on December 14, 1992; (B) computed values on December 14, 1992; (C) measured values on December 30, 1996 (new steady state for tunnel-disturbed conditions); (D) computed values in December 30, 1996; (E) nodes of the Finite Element Grid lying at the water table which were used to interpolate the watertable maps in panels (B) and (D); (F) Location of surface-drilled boreholes on the Äspö island used to interpolate measured watertable maps in panels (A) and (B). Computed contour maps include also a plain view of the tunnel trace.

polations correspond to those zones where there are no observation boreholes (Fig. 13G). Except for these two zones of the island without boreholes, computed and measured water table maps agree for the most part. This allows us to state that the actual water table is likely to be more irregular than that inferred from interpolation of available measured data. Maximum values of both measured and computed drawdowns after tunnel excavation are around 100 m. It is also worth noting that both measured and computed maps indicate that drawdowns are almost negligible on the northwestern part of the island, where there are no outcrops of the fracture zones.

7. Discussion

Calibrated values of hydraulic conductivities and storativities lie within the range of measured values. Fig. 14 shows a comparison of calibrated hydraulic conductivities and field-estimated values for each fracture zone. For the most part, calibrated values are within the range of field determinations. Fracture zones 5 and 15 (NE-1 and NNW-7, respectively) have calibrated conductivities which are slightly smaller than measured values (Fig. 14).

The fact that the model is able to reproduce accurately the observed tunnel inflows into control sections (Fig. 7) is the result of:

(a) The availability of a sound conceptual model for groundwater flow, which includes a comprehensive knowledge of the major water-conducting fracture zones.
(b) A proper calibration of fracture transmissivities and storativities. As mentioned before, calibrated parameters lie within the range of field measurements.
(c) An accurate simulation of the transient tunnel front advance by means of a time-varying boundary condition along the tunnel.

One of the major assumptions of the model is that it disregards the role of rock blocks between fracture zones. This assumption is responsible for the underestimation of the total amount of water flux into the

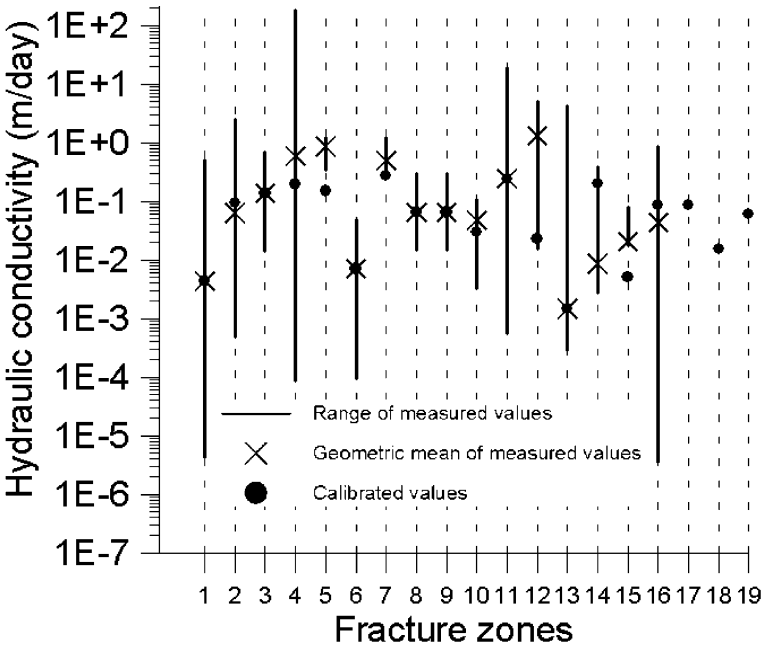

Fig. 14. Comparison of calibrated and measured fracture zone conductivities. Measurements show a wide scatter. For comparison purposes, the range of measured values and their geometric mean are indicated for each fracture zone. The starting guesses for the numerical model were the geometric mean values of field estimations (see Table 1 for fracture zone numbers).

tunnel (Fig. 8). Inasmuch as computed inflows match well measured flow rates at tunnel sections containing fracture zones, the observed discrepancies in the cumulative water inflow can be attributed to the hydrogeological role of the rock blocks. Discrepancies between measured and computed total inflows are due to water inflows that take place through tunnel sections which contains no major fracture zones. During the transient stage these sections contribute up to 20% of the total flow rate. This contribution decreases to less than 5% once steady-state is reached. This analysis indicates that rock blocks between major fracture zones have a noticeable storage capacity but a small transmissivity. On the other hand, neglecting the rock blocks in the model leads to an important saving of computational resources that can be used to simulate accurately the transient hydraulic response induced by the construction of the tunnel.

Our proposed numerical approach improves the capabilities of available analytical solutions to predict groundwater inflows into tunnels. Fig. 15 shows a comparison of tunnel inflows obtained with the analytical solution of Goodman et al. (1965) (Eq. (1)) and the numerical model. Both, numerical and analytical results have been plotted against available water inflows measured at the 14 control sections within the tunnel. It can be seen in Fig. 15 that the analytical solution overestimates tunnel inflows in several tunnel sections. This is mainly due to two reasons. On one hand, the analytical expression was derived for a semi-infinite aquifer with a constant head boundary on the top surface (Goodman et al., 1965). This assumption is clearly inappropriate for the fractured granites of the Äspö island where a significant drawdown was produced by tunnel construction. On the other hand, the spiral part of the Äspö HRL tunnel (Figs. 1 and 2) intersects several fracture zones more than once at different depths. This produces the interference of several radius of influence in those fracture zones being intersected by the spiral part of the tunnel. Goodman et al. (1965) solution does not account for such interferences.

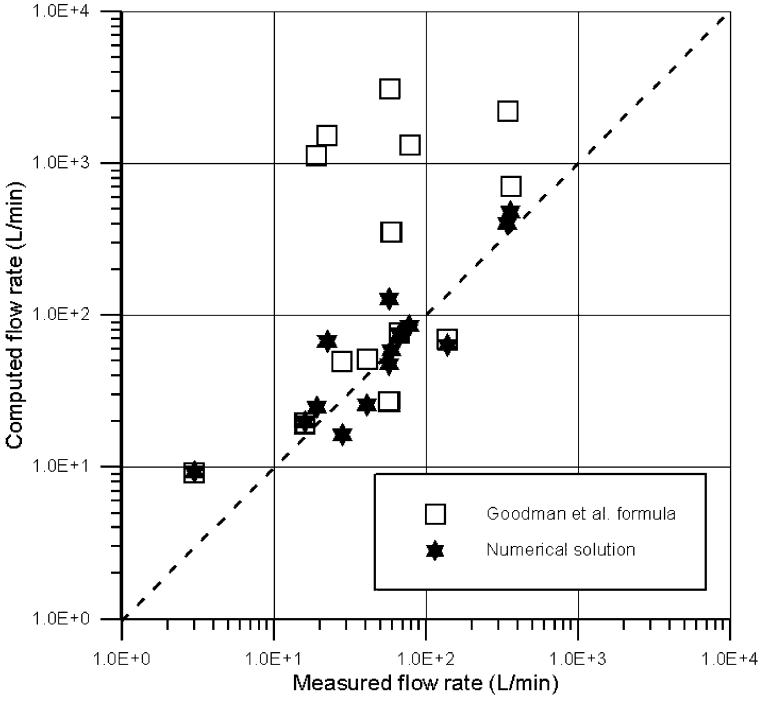

Fig. 15. Comparison of groundwater inflows computed by using the numerical model and the analytical solution of Goodman et al. (1965). Measured flow rates are also included in the plot.

8. Conclusions

A numerical methodology for the accurate dynamic simulation of the hydrogeological transient conditions induced by the construction of a tunnel has been presented. The methodology is based on the use of a Cauchy boundary condition at the nodes lying along the tunnel. This methodology has been implemented in a finite element code for groundwater flow in 3D fractured media (TRANMEF-3). The proposed methodology allows one to simulate the tunnel construction process without having to solve a set of concatenated computer runs or resort to the use of mobile grids. It has been used to simulate the impact of a tunnel construction on the groundwater system at the Äspö island (Sweden) which was constructed to access an underground research laboratory. The large amount of data available at this site provides a unique opportunity to test the performance of the numerical model and the proposed methodology for tunnel advance. After minor calibration, the numerical groundwater flow model of Äspö reproduces accurately both measured tunnel inflows and hydraulic heads at 30 control points by using calibrated parameter values, which are within the range of measured data. A validation exercise made by comparing model predictions and field data not used for calibration shows that the numerical model maintains in the validation stage a similar accuracy as in the calibration period. In addition, the numerical model has provided additional insight into the hydrogeology of the Äspö site by revealing that rock blocks between major water-conducting fracture zones show a noticeable storage capacity, but a small transmissivity. This may be the result of a poor connectivity of meso-scale fracture networks within rock blocks. By neglecting the role of rock blocks, our proposed modeling approach underestimates the transient cumulative water inflow into the total tunnel length by around 20%. This discrepancy decreases to less than 5% at steady state. This approach improves the capabilities of available analytical solutions and provides an efficient methodology to predict tunnel inflows at major fracture zones and drawdowns in the tunnel vicinity. From an engineering point of view, the proposed methodology leads to a significant saving in computational resources. From the numerical model of the Äspö site it can be concluded that a good hydrogeological characterization of large-scale conductive features should make possible to predict accurately the transient hydrogeological responses produced by tunneling works in fractured bedrocks.

Acknowledgements

This work has been carried out within the framework of Research Projects funded by ENRESA (Validation Project-703334), the RADWAS Program of the European Union (FEBEX I Project, FI4W-CT95-00008; FEBEX II Project, FIKW-CT-2000-0016) and by the Spanish Scientific and Technological Commission (HID98-0282). The Spanish Ministry of Science and Education and the Barrié de la Maza Foundation awarded research fellowships to the first and third authors, respectively. Access to the Äspö database was provided within the framework of the collaborative agreement between ENRESA and SKB. The authors want to thank SKB and all the people involved in the Äspö Task #5 for their support and fruitful discussions. Thanks are especially given to the external reviewers of the Project, Adrian Bath and Peter Jackson, for their thoughtful and relevant comments and suggestions.

References

Banwart, S., Gustafsson, E., Laaksoharju, M., 1999. Hydrological and reactive processes during rapid recharge to fracture zones. The Äspö large scale redox experiment. Appl. Geochem. 14, 873–8927.

Bear, J., 1993. Modeling flow and contaminant transport in fractured rocks. In: Bear, J., Tsang, C.F., de Marsily, G. (Eds.), Flow and Contaminant Transport in Fractured Media. Academic Press, San Diego, CA, pp. 1–37, Chap. 2.

Bear, J., Zalavsky, D., Irmay, S., 1968. Hydraulics of wells. Physical Principles of Water Percolation and Seepage. UNESCO, Paris, pp. 395–434, Chap. 13.

Berkowitz, B., 1994. Modeling flow and contaminant transport in fractured media. In: Corapcioglu, M.Y. (Ed.), Advances in Porous Media. Elsevier, Amsterdam, pp. 397–451, Chap. 6.

Carrera, J., Heredia, J., Vomvoris, S., Hufschmied, P., 1990. Fracture flow modeling: application of automatic calibration techniques to a small fractured monzonitic gneiss block. In: Neumann, S.P., Neretnieks, I. (Eds.), Hydrogeology of Low Permeability Environments. Hydrogeology Selected Papers, vol. 2. Int. Assoc. Hydrogeol. Verlag Heinz Heise, Hannover, pp. 169–194.

Custodio, E., 1983. Hidraulica de captaciones de agua subterránea. In: Custodio, E., Llamas, M.R. (Eds.), Hidrología Subterránea. Ediciones Omega, Barcelona, pp. 614–695 (In Spanish).

Freeze, R.A., Cherry, J.A., 1979. Groundwater. Prentice-Hall, New Jersey, 604 pp.

Galperin, A.M., Zaytsev, V.S., Norvatov, Y.A., 1993. Hydrogeology and Engineering Geology. Balkema, Rotterdam, 367 pp.

Goodman, R.D., Moye, S.A., Javandel, I., 1965. Groundwater inflows during tunnel driving. Eng. Geol. 2, 39–56.

Hautojärvi, A., Koskinen, L., Löfman, J., 1994. Hydraulic modeling of the large-scale redox experiment at Äspö HRL. In: Gustaffson, E. (Ed.), Hydraulic Modeling and Tracer Tests on the Redox Experiment in the Äspö Hard Rock Laboratory Tunnel. SKB Progress Report 25-94-37. Stockholm, SKB.

Jansson, G., 1979. Problems associated with heavy water leakage during construction of large area tunnels in granite, limestone and chalk. In: Katmura, I. (Ed.), Proc. Int. Tunnel Symp, pp. 187–192.

Juanes, R., 1997. Un código para la modelización tridimensional de flujo y transporte. Master thesis, ETS Ingenieros de Caminos, Canales y Puertos, University of A Coruña, A Coruña, Spain (In Spanish).

Juanes, R., Samper, J., 2001. Una formulación general y eficiente de fracturas en el M.E.F.: II. Aplicación a casos sintéticos. Rev. Int. Métodos Numer. Calculo Diseño Ing. 17 (1), 67–82 (In Spanish).

Juanes, R., Samper, J., Molinero, J., 2001. A general and efficient formulation of fractures and boundary conditions in the finite element method. Int. J. Numer. Methods Eng. (Submitted).

Kiraly, L., 1987. Large scale 3-D groundwater flow modeling in highly heterogeneous geologic medium. In: Custodio, E., et al. (Eds.), Groundwater Flow and Quality Modeling. D. Reidel Publishing, Dordrecht, Holland, pp. 761–775.

Kornfalt, K.A., Wikman, H., 1988. The rocks of the Äspö island. Description of the detailed maps of solid rocks including maps of 3 uncovered trenches, SKB Progress Report 25-88-12. Stockholm.

Larson, S.A., Berglund, J., 1992. A geochronological subdivision of the Transscandinavian Igneous Belt—three magmatic episodes. Geol. Foeren. Stockhlom Foerh. 114, 459–461.

Molinero, J., 2000. Testing and validation of numerical models of groundwater flow, solute transport and chemical reactions in fractured granites. A quantitative study of the hydrogeological and hydrochemical impact produced by the construction of the Äspö Underground Laboratory (Sweden). PhD dissertation, Department of Construction Technology. University of A Coruña, Spain. 221 pp. (without appendices).

Molinero, J., Samper, J., Juanes, R., Bujan, L., 2000. Impact of the tunnel construction on the groundwater system at Äspö. Final Report. Äspö Task Force Interim Report. University of A Coruña, Spain, 119 pp.

Rhén, I., Bäckbom, G., Gustafson, G., Stanfors, R., Wikberg, P., 1997a. Results from pre-investigations and detailed site characterization, Summary Report. SKB Technical Report 97-03. Stockholm.

Rhén, I., Gustafson, G., Stanfors, R., Wikberg, P., 1997b. Models based on site characterization 1986–1995. SKB Technical Report 97-06. Stockholm.

Smellie, J.A.T., Laaksoharju, M., Wikberg, P., 1995. Äspö, SE Sweden: a natural groundwater flow model derived from hydrochemical observations. J. Hydrol. 172, 145–169.

Stanfors, R., Rhén, I., Tullborg, E.L., Wikberg, P., 1999. Overview of geological and hydrogeological conditions of the Äspö Hard Rock Laboratory site. Appl. Geochem. 14, 819–834.

Ström, A., 1996. The Äspö task force on modeling of groundwater flow and transport of solutes. In: Hammarström, M., Olsson, Ö. (Eds.), Äspö Hard Rock Laboratory. 10 Years of Research. SKB, Stockholm, pp. 47–50.

Wikberg, P., 1998. Plan for Modeling Task #5: Impact of the Tunnel Construction on the Groundwater System at Äspö: A Hydrological–Hydrochemical Model Assessment Exercise. SKB Progress Report HRL-98-07. Stockholm, 12 pp.